Efficient Linear Time-Varying System Identification Using Chirp Waveforms

Andrew Harms*[1], Waheed Bajwa†[2], Robert Calderbank*[3]
*Department of Electrical and Computer Engineering, Duke University, Durham, NC, USA
†Department of Electrical and Computer Engineering, Rutgers University, Piscataway, NJ, USA
[1]andrew.harms@duke.edu [2]waheed.bajwa@rutgers.edu [3]robert.calderbank@duke.edu

***Abstract*—Linear, time-varying (LTV) systems are operators composed of time shifts, frequency shifts, and complex amplitude scalings that act on continuous finite-energy waveforms. This paper builds upon a novel, resource-efficient method previously proposed by the authors for identifying the parametric description of such systems from the sampled response to linear frequency modulated (LFM) waveforms. If the LTV operator is probed with a sufficiently diverse set of LFM pulses, more LFM pulses than reflectors, then the system can be identified with high accuracy. The accuracy is shown to be proportional to the uncertainty in the estimated frequencies and confirmed with numerical experiments.**

I. Introduction

Linear, time-varying (LTV) systems are systems that act on input signals and produce an output signal that is time-shifted, frequency-shifted, and scaled by a complex amplitude. LTV systems easily lend themselves to a parametric description in terms of the time and frequency shifts and amplitude scalings. Identifying such systems involves recovering this parametric description. LTV system identification has applications in active sensing, such as radar or sonar, and channel estimation for communication systems, among other areas. This paper concentrates on the radar setting to make the ideas more concrete, but the reader should keep in mind that the framework is more general.

A major challenge in LTV system identification, especially in the active sensing application, is the efficient recovery of the parametric description, i.e., the estimation of the time shifts, frequency shifts, and amplitude scalings. We will focus on two primary areas of performance: 1) estimation accuracy, and 2) efficiency in terms of physical resource usage. For the latter, we primarily focus on two physical resources: required sampling rate of the receiver and the time-bandwidth resources required of the probing waveform.

Several approaches have been proposed to solve the LTV system identification problem. Traditional radar processing uses a matched filter where the LFM returns are correlated against a reference LFM waveform, or slight variations of this process [1]. The primary advantage to such an approach is the efficient implementation using FFT algorithms. The primary disadvantage is the limited resolution offered due to the inherent windowing in the FFT. More recent approaches have proposed the use of compressed sensing and/or parametric estimation techniques. One such approach discretizes the parameter space so that compressed sensing recovery techniques can be applied to a small number of acquired samples of the system response [2]. Another pair of approaches use similar parametric techniques that do not require discretizing the parameter space. One uses phase-coded pulses as a probing waveform and recovers the time shifts first, followed by the frequency shifts [3]. The second uses frequency-stepped pulses to recover the frequency shifts, followed by the time shifts [4]. We recently proposed the technique addressed in this paper that uses linear frequency modulated (LFM) pulses and recovers the time shifts and frequency shifts simultaneously [5].

A. Our Contributions

The primary focus of this paper is on the design of the probing waveform to make the time-bandwidth product small. The LFM pulses we are using as probing waveforms are described in Section II-A. To make the time-bandwidth product small, we want to estimate the parameters of the LTV system description using as few pulses as possible. Therefore, it is important to understand how the choice of LFM waveforms affects the parameter estimation. To that end, we provide two results that show that a sufficiently diverse set of LFM pulses can unambiguously recover the parametric description. The first result is asymptotic in nature and shows perfect recovery if enough pulses are used. The second result shows that the accuracy of the recovery with a finite number of pulses is on the order of the variance of the frequency estimator as long as a sufficient number of pulses are used with sufficiently diverse LFM parameters.

II. Response of LTV Systems to LFM Pulses

An LTV system, shown in Fig. 1, is an operator that acts on a *probing waveform* $x(t)$ and consists of K amplitude-scaled time shifts and frequency shifts. The response of the system to a probing signal $x(t)$ has the parametric description

$$y(t) = \sum_{k=1}^{K} c_k x(t-\tau_k) e^{j2\pi f_k t} + \varepsilon(t) \tag{1}$$

for $t \in [0, \mathcal{T}]$ where $\mathcal{T}$ is the processing interval, during which the parameters are assumed fixed. Each component of the sum, indexed by k and referred to as a *reflector* return, is parameterized by a distinct triplet (τ_k, f_k, c_k) corresponding to the time shift, frequency shift, and complex amplitude of each reflector. We assume that $f_k \in (-f_{\max}, f_{\max})$, $\tau_k \in [0, \tau_{\max})$, and $c_k \in \mathbb{C} \setminus \{0\}\ \forall k$. The term $\varepsilon(t)$ is a noise term corrupting

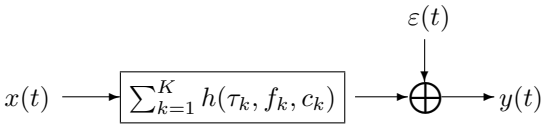

Fig. 1: Block diagram of the LTV system (1). A probing signal is time and frequency shifted prior to the addition of noise.

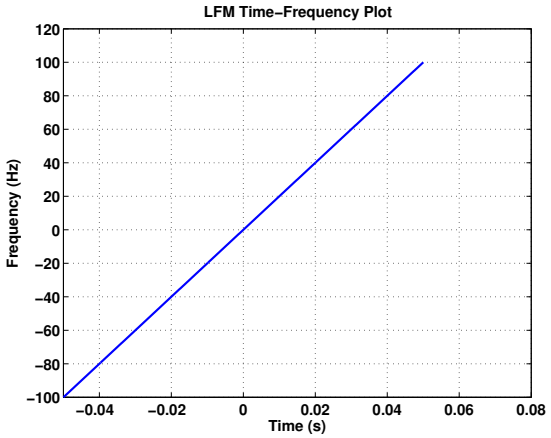

Fig. 3: Time-frequency depiction of an LFM pulse with $T_p = 0.1$ and $f_c^m = 2000$. The frequency sweeps linearly with time.

the response. In this paper, this noise term will be assumed to be additive white Gaussian noise (AWGN) with variance σ^2.

A. LFM Probing Waveform

Linear frequency modulated (LFM) pulses are constant amplitude pulses with frequency that linearly sweeps across some bandwidth. Consider a train of M such pulses

$$x(t) = \sum_{m=0}^{M-1} x_m(t - mT)$$

with

$$x_m(t) = e^{j2\pi f_c^m t^2} g(t)$$

and window function $g(t) = 0$ for $t \notin [0, T_p]$. Each LFM pulse sweeps across a bandwidth $f_c^m \cdot T_p$, as shown in Fig. 3. We also require that $T > T_p$, so that there is a guard interval of $T_g = T - T_p > \tau_{\max}$ between transmitted pulses. This ensures that the returns from each pulses can be separated at the receiver. See Fig. 4 for a graphical summary.

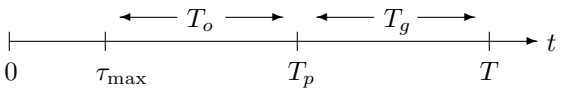

Fig. 4: Timing diagram of a single LFM pulse. If $T_g = T - T_p > \tau_{\max}$ and $T_p > \tau_{\max}$, then the pulses do not overlap and a measurement period $T_o = T_p - \tau_{\max}$ is guaranteed to contain returns from each reflector.

B. Receiver Processing

We provide a brief summary of the receiver processing to set the context of our main results. For a more thorough explanation, please see [5]. Each received pulse is filtered, dechirped, and sampled at a rate $f_s \geq 2(f_{\max} + 2f_c^m \tau_{\max})$ as shown in Fig. 2a. This procedure is similar to *stretch processing*, a traditional radar processing technique [6]. The resulting signal is a sum of sinusoids

$$\tilde{y}_m[n] = \sum_{k=1}^{K} c_k e^{j2\pi\theta_k^m} e^{j2\pi\nu_k^m n T_s} + \tilde{\varepsilon}[n]$$

with frequencies

$$\nu_k^m = f_k - 2f_c^m \tau_k. \tag{2}$$

The noise term $\tilde{\varepsilon}[n]$ consists of AWGN samples with variance σ^2.

The samples from each pulse $\tilde{y}_m[n]$ are used as input to a spectral estimation algorithm. We stress that there is considerable flexibility in the choice of algorithm, and a comparison is beyond the scope of this paper. Some possible choices include MUSIC, ESPRIT, or Fourier techniques, such as an FFT followed by a peak detector. In the simulations provided below, we chose the Kumaresan-Tufts (KT) algorithm [7]. After recovering the frequencies ν_k^m from each pulse, these frequencies are fed into a matching algorithm, as shown in Fig. 2b. We describe the *Matching Procedure* block in the next section.

III. Recovering the LTV Description

The LTV system identification problem consists of two separate pieces: the detection of (the number of) reflectors, and the estimation of the reflector parameters. The distinction between these two pieces can sometimes be blurred or these can be performed simultaneously. In the context of parametric recovery, the detection problem boils down to estimating K, the number of reflectors. This problem has been addressed extensively in the literature in the context of different algorithms, e.g., [8]–[10]. The key insight is that the measurements can be separated into a signal subspace and an orthogonal noise subspace. For example, if the noise is not too large then the eigenvalues or singular values will be separated into two groups corresponding to these two subspaces. The details are beyond the scope of this paper. With an estimate of K, or with oracle knowledge of K, we use the KT algorithm to produce frequency estimates $\hat{\nu}_k^m$ in the *Spectral Estimation* blocks.

To describe the matching algorithm, we first need to set up some notation. The LTV parameters are collected into a vector

$$\beta = [f_1, \ldots, f_K, \tau_1, \ldots, \tau_K]^T.$$

The chirp rates are collected into a matrix, which captures the constraints on the frequencies (2), and is given by

$$\mathbf{A}(M) = \begin{bmatrix} 1 & -2f_c^1 \\ \vdots & \vdots \\ 1 & -2f_c^M \end{bmatrix} \otimes \mathbf{I}_K$$

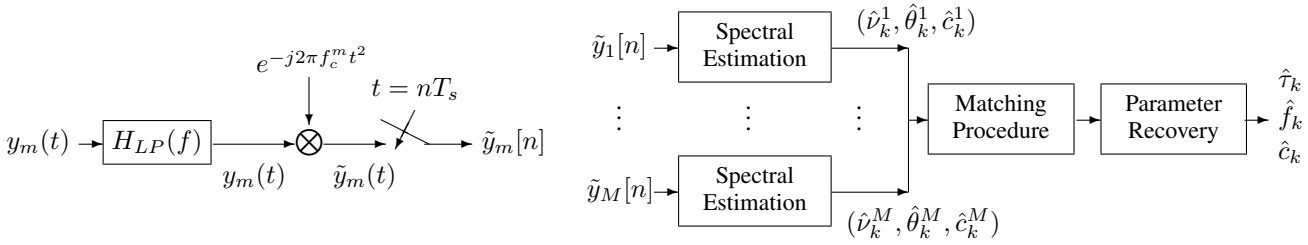

(a) Analog processing

(b) Digital processing

Fig. 2: Processing block diagrams.

with the notation emphasizing the dependence on M. Note that $\mathbf{A}(M)$ is full rank as long as all the chirp rates are not the same. The recovered frequency from each pulse are collected into a vector

$$\hat{\nu}(M) = [\hat{\nu}_1^1, \ldots, \hat{\nu}_K^1, \hat{\nu}_1^2, \ldots, \hat{\nu}_K^2, \ldots, \hat{\nu}_1^M, \ldots, \hat{\nu}_K^M]^T.$$

A block diagonal permutation matrix $\mathbf{P}(M)$ determines the ordering of the recovered frequencies from each pulse. Each block along the diagonal is a $K \times K$ permutation matrix. If the frequency estimates $\hat{\nu}_k^m$ are perfect and have no error, then the reflector parameters β can be found via the solution to

$$\mathbf{A}(M)\beta = \mathbf{P}(M)\hat{\nu}(M). \tag{3}$$

Here, $\mathbf{A}(M)$ is the set of design parameters, $\hat{\nu}(M)$ are the inputs (derived from the measured response), and $\mathbf{P}(M)$ and β make up the search space for the solution. If M is large enough, then there is a unique solution to (3) that determines the reflector parameters.

A. Disambiguating Targets

In the case of noisy measurements, which lead to errors in the recovered frequencies, a least-squares type of problem is more appropriate. The reflector parameters can be recovered via the following optimization

$$\hat{\beta}(M) = \arg\min_{\beta} \min_{\mathbf{P}(M)} ||\mathbf{A}(M)\beta - \mathbf{P}(M)\hat{\nu}(M)||_2^2. \tag{4}$$

For a given permutation matrix $\mathbf{P}(M)$ and full rank $\mathbf{A}(M)$, the MMSE parameter vector, i.e., the minimizer of (4) over β, is given by the pseudoinverse (the M is dropped from the notation when the context makes it apparent)

$$\hat{\beta}(M, \mathbf{P}) = (\mathbf{A}^*\mathbf{A})^{-1}\mathbf{A}^*\mathbf{P}\hat{\nu}(M).$$

The permutation matrix $\mathbf{P}(M)$ that minimizes (4) will determine the correct set of reflector parameters if the corresponding noiseless problem is not underdetermined. Otherwise, we have ambiguous matchings.

Before stating our main results, we want to build intuition into how the choice of pulse parameters f_c^m affects the solution to (4). Consider Fig. 5 where we have plotted the constrains that result from four pulses with chirp rates ± 2000 Hz/s and ± 4000 Hz/s. The true reflector parameters are marked with blue circles in both plots, and the constraints from the positive chirp rates are plotted in black while the constraints

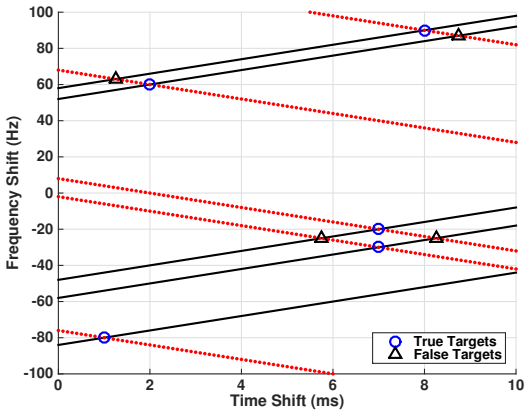

(a) Line constraints for $f_c = 2000$ Hz/s.

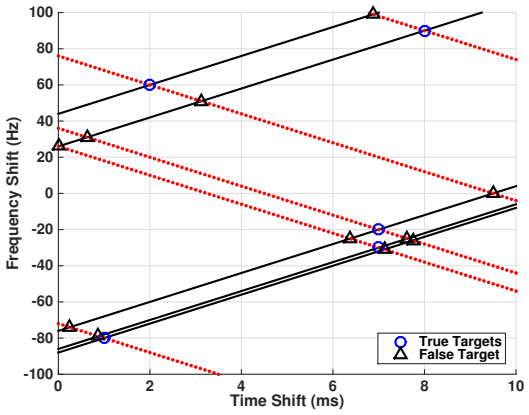

(b) Line constraints for $f_c = 4000$ Hz/s.

Fig. 5: Line constraints for two pulses.

from the negative chirp rates are plotted in red. Each set of true reflector parameters are coincident with intersections of the lines corresponding to these constraints. Notice in each plot, however, that there are other solutions shown by black triangles that satisfy the constrains from two pulses. If both plots are considered together, the blue circles are the only common solutions that satisfy all 4 constraints. In the case of perfect frequency recovery, it is straightforward to show that (3) has a unique solution if $M > K$.

If the frequency recovery contains errors due to noisy mea-

surements, then an additional requirement on the separation of the chirp rates is required. This can be visualized by thinking of the lines in the plots of Fig. 5 having some thickness directly related to the uncertainty in the frequency estimates. The problem no longer has a perfect solution, and hence the need for the least-squares criterion. We state this formally in the next subsection.

B. Choosing Sufficiently Diverse Pulse Parameters

We present two results that show we can disambiguate the reflector returns if the frequency estimates are imperfect. In each, we concentrate on the optimization (4). The first result is asymptotic and shows that we can recover the parameters with perfect accuracy if we choose every LFM pulse with a different chirp rate f_c^m.

Theorem 1 (Asymptotically Perfect Recovery)**.** *Fix τ_{max} and f_{max} and choose $f_c^a \neq f_c^b$ for $a \neq b$. Take the samples $\tilde{y}_m[n]$ for $m = 1, \ldots, M$ with $f_s \geq 2(f_{\max} + 2\max_m(f_c^m)\tau_{\max})$ as input to a frequency estimator to produce estimated frequencies $\hat{\nu}_k^m$. The solution to*

$$\hat{\beta}(M) = \arg\min_{\beta} \min_{\mathbf{P}(M)} ||\mathbf{A}(M)\beta - \mathbf{P}(M)\hat{\nu}(M)||_2^2$$

converges in probability to the true parameters as $M \to \infty$, i.e.,

$$\hat{\beta}(M) \to \beta.$$

The proof is found in [5] and relies on the law of large numbers. The second result says that if we choose the LFM chirp rates with separation larger than the error from the frequency estimator, and we have as many LFM pulses as reflector detections K, then we can perfectly disambiguate the detections and the estimation error is proportional to the frequency estimation error.

Theorem 2 (Sufficient Diversity of LFM Pulses)**.** *Fix τ_{max} and f_{max} and choose $f_c^m = f_c^{m-1} + \mathrm{C}$ for $m = 2, \ldots, M$. Take the samples $\tilde{y}_m[n]$ for $m = 1, \ldots, M$ with $f_s \geq 2(f_{\max} + 2\max_m(f_c^m)\tau_{\max})$ as input to an unbiased frequency estimator that produces Gaussian distributed estimated frequencies $\hat{\nu}_k^m$. If $\mathrm{C} \geq Var(\hat{\nu}_k^m)$, $M > K$, and $M > 2$, then the solution to*

$$\hat{\beta}(M) = \arg\min_{\beta} \min_{\mathbf{P}(M)} ||\mathbf{A}(M)\beta - \mathbf{P}(M)\hat{\nu}(M)||_2^2$$

satisfies

$$\mathbb{E}||\hat{\beta}(M) - \beta||_2^2 \leq \mathrm{B}\frac{Var(\hat{\nu}_k^m)}{M}.$$

The constant B depends on the estimator used. We omit the proof in the interest of space, but will provide it in a forthcoming journal article. To build intuition on Theorem 2, consider the constraints illustrated in Fig. 6. These are similar to all four constraints shown in Fig. 5, but with the reflector parameters changed slightly to illustrate an unresolved ambiguity. Here we have 4 LFM pulses and 5 reflectors whose true parameters are shown with blue circles. The reflector parameters and LFM chirp rates were chosen in such a way that a set of parameters,

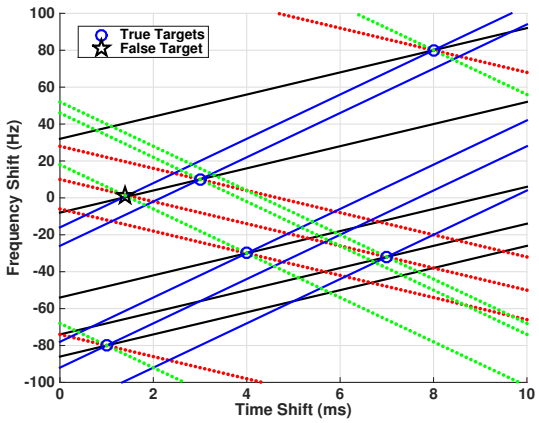

Fig. 6: Line constraints for $f_c = 2000, 4000$ Hz/s and 5 targets.

shown by the black star, also satisfy these 4 sets of constraints. If $M > K$ and $M > 2$, then there are only K such points that satisfy all M constraints because there are not sufficient degrees of freedom in the choice of reflector parameters.

As for intuition into the effect of the estimated frequency uncertainty, consider the same scene as in Fig. 6 with estimated five reflectors shown by the blue circles. The matching procedure would recover these sets of parameters, but the estimator uncertainty means that there is a region around each that is likely to contain the true target parameters. The shape of this region is an intersection of diamond shapes due to each pair of constraints (given by the chirp rates). If two (or more) of these regions are overlapping, then we cannot reliably separate the two reflectors in the parameter space. As more pulses are used to further constrain the problem, we are shrinking the area covered by this uncertainty. The constant C ensures that each area of uncertainty for each reflector is non overlapping.

IV. Numerical Experiments

To confirm that the optimization (4) produces accurate estimates, we performed numerical experiments using the KT algorithm [7] to perform the frequency recovery on measurements corrupted with AWGN of variance $\sigma^2 = 0.01$. The result is shown in Fig. 7 using four LFM pulses with chirp rates $f_c = \pm 2000, \pm 4000$. In addition, we performed Monte Carlo simulations over 1000 random realizations of 5 sets of reflector parameters and noise realizations for a range of noise variances. The average error from these trials is shown in Fig. 8 where the SNR is the ratio of the energy of each target to the noise energy on a dB scale.

V. Conclusions

In conclusion, we have built upon the method proposed in [5] and presented non asymptotic criteria for choosing the number of pulses and the pulse parameters in order to successfully identify an LTV system. The number of pulses must be larger than the number of reflectors, and the chirp rates of the pulses must be separated by at least the variance of the frequency estimates. If this is the case, then the

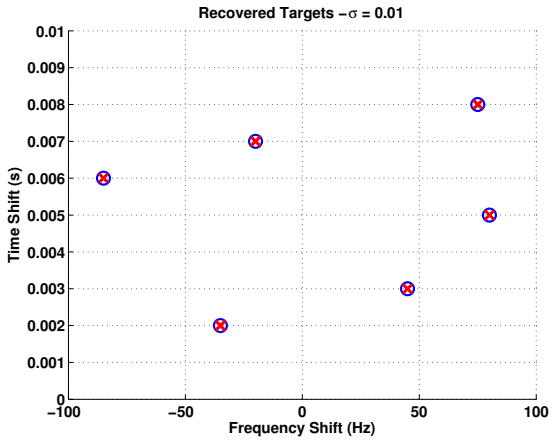

Fig. 7: Estimation of reflector parameters with AWGN $\sigma^2 = 0.01$. The true reflector parameters are shown by a blue circle while the recovered parameters are shown by a red x.

optimization (4) recovers the LTV system with an accuracy that is proportional to the variance of the frequency estimates.

REFERENCES

[1] M. Skolnik, *Radar handbook*, 3rd ed. New York: McGraw-Hill, 2008.

[2] M. Herman and T. Strohmer, "High-resolution radar via compressed sensing," *IEEE Trans. Sig. Proc.*, 2009.

[3] W. U. Bajwa, K. Gedalyahu, and Y. Eldar, "Identification of parametric underspread linear systems and super-resolution radar," *IEEE Trans. Sig. Proc.*, 2011.

[4] B. Friedlander, "An efficient parametric technique for doppler-delay estimation," *IEEE Trans. Sig. Proc.*, vol. 60, no. 8, 2012.

[5] A. Harms, W. U. Bajwa, and R. Calderbank, "Identification of linear time-varying systems through waveform diversity," *arXiv:1410.3786*, 2014.

[6] D. Barton, *Radar System Analysis*. Prentice-Hall, 1964.

[7] D. W. Tufts and R. Kumaresan, "Estimation of frequencies of multiple sinusoids: Making linear prediction perform like maximum likelihood," *Proc. IEEE*, vol. 70, no. 9, pp. 975–989, 1982.

[8] ——, "Singular value decomposition and improved frequency estimation using linear prediction," *IEEE Trans. Acoust., Speech, Signal Proc.*, vol. 30, no. 4, pp. 671–675, 1982.

[9] R. Kumaresan, D. W. Tufts, and L. Scharf, "A prony method for noisy data: Choosing the signal components and selecting the order in exponential signal models," *Proc. IEEE*, vol. 72, no. 2, pp. 230–233, 1984.

[10] J. Thomas, L. Scharf, and D. W. Tufts, "The probability of a subspace swap in the SVD," *IEEE Trans. Sig. Proc.*, vol. 43, no. 3, pp. 730–736, 1995.

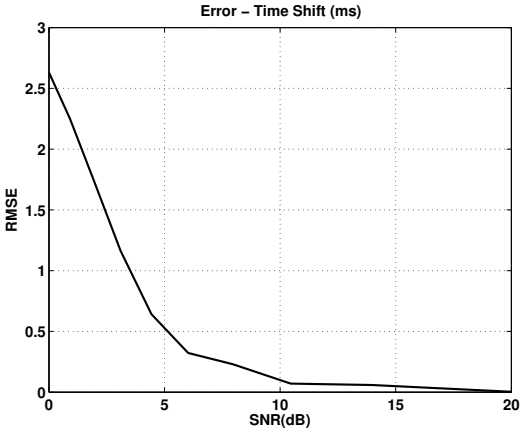

(a) Time shift error

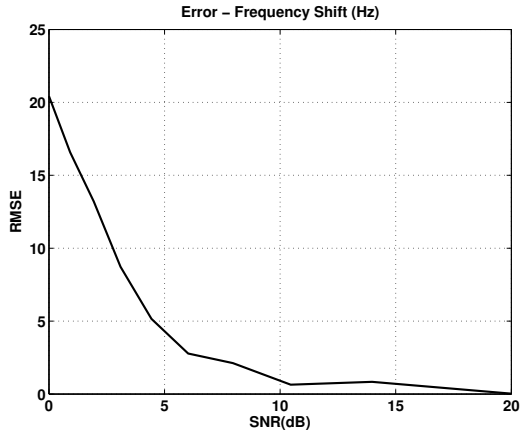

(b) Frequency shift error

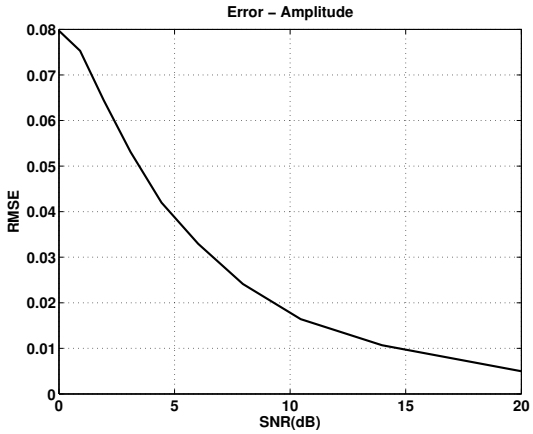

(c) Amplitude error

Fig. 8: Recovery error from noisy measurements over 1000 Monte Carlo trials. Note the threshold at ≈ 10 dB below which the error increases rapidly. This effect is due to the parametric frequency estimator.